The Journal of Chemical Physics

RESEARCH ARTICLE | NOVEMBER 27 2023

A density functional theory and simulation study of stripe phases in symmetric colloidal mixtures

Santi Prestipino ; Davide Pini ; Dino Costa ; Gianpietro Malescio ; Gianmarco Munaò

J. Chem. Phys. 159, 204902 (2023)
https://doi.org/10.1063/5.0177209

The Journal of Chemical Physics ARTICLE pubs.aip.org/aip/jcp

A density functional theory and simulation study of stripe phases in symmetric colloidal mixtures

Cite as: J. Chem. Phys. 159, 204902 (2023); doi: 10.1063/5.0177209
Submitted: 20 September 2023 • Accepted: 30 October 2023 •
Published Online: 27 November 2023

Santi Prestipino,[1] Davide Pini,[2] Dino Costa,[1] Gianpietro Malescio,[1] and Gianmarco Munaò[1,a)]

AFFILIATIONS

[1] Dipartimento di Scienze Matematiche e Informatiche, Scienze Fisiche e Scienze della Terra, Università degli Studi di Messina, Viale F. Stagno d'Alcontres 31, 98166 Messina, Italy

[2] Dipartimento di Fisica "A. Pontremoli," Università di Milano, Via Celoria 16, 20133 Milano, Italy

[a)] **Author to whom correspondence should be addressed:** gianmarco.munao@unime.it

ABSTRACT

In a binary mixture, stripes refer to a one-dimensional periodicity of the composition, namely, a regular alternation of layers filled with particles of mostly one species. We have recently introduced [Munaò *et al.*, Phys. Chem. Chem. Phys. **25**, 16227 (2023)] a model that possibly provides the simplest binary mixture endowed with stripe order. The model consists of two species of identical hard spheres with equal concentration, which mutually interact through a square-well potential. In that paper, we have numerically shown that stripes are present in both liquid and solid phases when the attraction range is rather long. Here, we study the phase behavior of the model in terms of a density functional theory capable to account for the existence of stripes in the dense mixture. Our theory is accurate in reproducing the phases of the model, at least insofar as the composition inhomogeneities occur on length scales quite larger than the particle size. Then, using Monte Carlo simulations, we prove the existence of solid stripes even when the square well is much thinner than the particle diameter, making our model more similar to a real colloidal mixture. Finally, when the width of the attractive well is equal to the particle diameter, we observe a different and more complex form of compositional order in the solid, where each species of particle forms a regular porous matrix holding in its holes the other species, witnessing a surprising variety of emergent behaviors for a very basic model of interaction.

I. INTRODUCTION

The emergence of complex motifs from simple interaction rules is a recurring issue—actually, one of paramount importance—in soft-matter physics.[1–4] A non-exhaustive list of materials where the formation of supramolecular structures occurs spontaneously at equilibrium includes colloids,[5–7] polymers,[8–10] amphiphilic systems,[11,12] liquid crystals,[13,14] and protein solutions.[15,16] During the last decades, much effort has been devoted to identify simple particle models where specific examples of self-assembly are realized, most notably the appearance of stripe patterns in multi-component systems, in which blocks of different chemical compositions and/or experiencing different intermolecular interactions alternate along a given direction. Stripes are experimentally observed, among others, in photonic crystals,[17] in Langmuir and lipid monolayers,[18,19] and in polymer nanocomposites.[20,21]

Due to the increasing importance of stripes for technological applications, a proper understanding of the microscopic mechanisms underlying their occurrence in systems of soft particles is crucial. A first possibility is to use a short-range interparticle attraction and a longer-range anisotropic repulsion, like in the venerable axial next-nearest neighbor Ising (ANNNI) model.[22] However, anisotropic forces are by no means necessary for generating stripes, since curved stripes are observed in systems of particles interacting through a fully isotropic core-corona potential.[23–26] Here, under suitable thermodynamic conditions, particles organize themselves into "lanes," ultimately arising as a trade-off between the two competing requirements of entropy maximization (which prompts the particles to pack efficiently) and energy minimization (which, rather, would keep them apart). Still different is the mechanism underlying the onset of stripes in SALR fluids, characterized by the simultaneous presence of isotropic short-range attraction (SA) and long-range repulsion (LR) between the particles.[27–31] While the SA promotes aggregation, a sufficiently strong LR rules out the possibility of liquid–vapor separation, encouraging the formation of separate aggregates of finite size. At sufficiently low

temperatures, such aggregates—which at low density are in the form of spheroidal clusters—can be arranged in a variety of different structures, including lamellar phases.[32–37]

Stripes have been investigated, though less extensively, also in binary mixtures, where they have been reported both in experiments[38,39] and in theoretical studies.[40–45] In a recent paper,[46] we introduced a model system that is admittedly the minimal binary mixture with stripe order, namely, an equimolar mixture of identical hard spheres endowed with a cross attraction of square-well (SW) type. For wells widths $\gamma\sigma$ wider than the sphere diameter σ, we have documented by Monte Carlo simulations the existence of planar stripes in the solid phase, finding that their thickness grows linearly with the attraction range. We have also seen stripes in the dense liquid as long as γ is large enough.

Rather counterintuitively, we have shown that in our mixture, stripe order arises when "like" interactions (i.e., between particles of the same species) are repulsive, whereas the cross (or "unlike") interaction is attractive beyond the core. As puzzling as the formation of extended domains of like particles due to a strong unlike attraction may seem, it is not difficult to realize how this can happen at high density using the following simple reasoning. When γ is sufficiently small, the SW attraction reaches only the first neighbors. In a fcc crystal with single-layer stripes oriented along [001], each particle has eight unlike neighbors (over a total of 12), while in the substitutionally disordered crystal, the average number of unlike neighbors is six. Therefore, the energy (and also the enthalpy) of the striped crystal is more negative. In other words, the formation of stripes is an emergent phenomenon driven by energy: planar stripes succeed in maximizing the number of attracting unlike spheres, making the striped configuration more stable than its compositionally disordered counterpart. Strangely enough, the above argument indicates that stripes are energetically preferred even when γ is close to zero, insofar as the temperature is low enough and the density is high.

In this paper, we highlight the significance and extent of stripe order in our mixture, again focusing on the equimolar case. First, we show that stripes can be predicted by a statistical theory rather than accounted for by numerical simulations alone. To this end, we provide a mean-field treatment of the mixture behavior expressed in the language of density functional theory (DFT). Within this framework, we offer a full justification for the existence of stripes in the dense mixture, predicting a phase diagram that is overall consistent with that obtained from simulation.[46] We also test the accuracy of two different analytic approximations: the first one is based on a sinusoidal ansatz for the density profile, which is suited to describe the striped fluid near the boundary with the homogeneous fluid. The second approximation, more appropriate in the high-density regime, schematizes the stripes as one-component layers separated by sharp interfaces. Then, we carry out extensive Monte Carlo (MC) simulations of the solid to probe the existence and nature of compositional order in mixtures with $\gamma \leq 1$, a range of values where our DFT is inadequate since the inhomogeneities in the composition occur on length scales comparable to the particle size. In particular, we confirm the existence of stripes for γ as small as 0.1, i.e., for conditions making our simplistic model more akin to a real colloidal mixture. Clearly, stripes can exist in the solid phase only when the temperature is not too high. By employing a suitably designed order parameter, we find that when the mixture is heated up, stripes disappear abruptly for $\gamma = 0.1$ and more smoothly for the other γ values examined. After a careful analysis, the case $\gamma = 1$ turns out to be special. At very high density, the most stable low-temperature solid is a hcp crystal with a compositional order different from stripe order, characterized by narrow bands of particles of one species intercalated with bands of the other species. By heating this system gradually at constant density, we observe a smooth transition to a striped hcp crystal until the latter order is washed out.

Our paper is organized as follows: in Sec. II, we present our DFT study of the mixture, discussing the relative stability of the various phases. In Sec. III, after describing the numerical tools needed to investigate liquid–vapor coexistence in simulation as well as the structural and compositional orders at high density, we discuss the results obtained for a few small values of γ. Conclusions and perspectives are outlined in Sec. IV. To facilitate reading, more technical considerations have been confined to two appendices.

II. DENSITY FUNCTIONAL THEORY

A. Grand-potential functional

We consider an equimolar mixture of two species of hard spheres (labeled 1 and 2) with equal diameter σ, which mutually interact through a SW potential u_{12} of range $(1+\gamma)\sigma$,

$$u_{12}(r) = \begin{cases} +\infty, & \text{if } r < \sigma, \\ -\varepsilon, & \text{if } \sigma \leq r < \sigma + \gamma\sigma, \\ 0, & \text{otherwise}, \end{cases} \tag{1}$$

where r is the interparticle distance. In the following, all quantities are expressed in reduced units such that σ is the length unit and ε is the energy unit. In Ref. 46, the phase behavior of this model was investigated by Monte Carlo simulations. We found that planar stripes are present in the cold solid for $\gamma \geq 1$. A zero-temperature analysis showed that, near close packing, the thickness of stripes grows linearly with γ. When γ is 2 or larger, blurred stripes are also present in the bulk liquid.

To obtain an independent, fully theoretical understanding of the mixture behavior, we resort to a DFT approximation that is as simple as possible. In the same spirit of the mean-field or Van der Waals approximation, we express the excess free-energy functional F^{exc}—depending on the number-density fields of the two species, $\rho_1(\mathbf{x})$ and $\rho_2(\mathbf{x})$—as the sum of a repulsive term, F_{rep}, and an attractive term, F_{attr}.

As for F_{rep}, this functional is taken to be of the local-density form

$$F_{\text{rep}} = \int \mathrm{d}^3x \, (\rho_1(\mathbf{x}) + \rho_2(\mathbf{x})) f_{\text{HS}}(\rho_1(\mathbf{x}) + \rho_2(\mathbf{x})), \tag{2}$$

where the integral is extended over the macroscopic volume V of the system and $f_{\text{HS}}(\rho)$ is the excess free energy per particle of a one-component fluid of hard spheres in the Carnahan–Starling approximation,

$$\beta f_{\text{HS}}(\rho) = \frac{\eta(4-3\eta)}{(1-\eta)^2} \quad \text{with} \quad \eta = \frac{\pi}{6}\rho\sigma^3. \tag{3}$$

As usual, $\beta = (k_B T)^{-1}$ denotes the inverse temperature in units of the Boltzmann constant. The rationale behind Eqs. (2) and (3) is

clear: in the absence of any attraction between the spheres [$\varepsilon = 0$ in Eq. (1)], the mixture becomes a fluid of indistinguishable hard spheres.

As for $F_{\rm attr}$, we set

$$F_{\rm attr} = \frac{1}{2}\sum_{i,j=1}^{2} \int {\rm d}^3x \int {\rm d}^3x'\, w_{i,j}(|\mathbf{x}-\mathbf{x}'|)\rho_i(\mathbf{x})\rho_j(\mathbf{x}'), \tag{4}$$

where $w_{i,i} = 0$ and

$$w_{12}(r) = w_{21}(r) = \begin{cases} -\varepsilon, & \text{if } r < \xi, \\ 0, & \text{otherwise,} \end{cases} \tag{5}$$

with $\xi = (1+\gamma)\sigma$. Equation (4) is equivalent to treating the cross attraction in the random phase approximation. Upon comparing w_{12} with u_{12}, we see that, at variance with Eq. (1), the attraction range in (5) has been extended down to zero distance.[34,47] Given that the potential u_{12} is infinitely repulsive inside the core, there is no compelling reason to prefer a different prescription for w_{12} in such a region. We chose the form in Eq. (5) since it offers the advantage of simplifying the formulas.

The grand-potential functional of the mixture is finally

$$\Omega = \Omega^{\rm id} + F^{\rm exc}, \tag{6}$$

with

$$\Omega^{\rm id} = k_BT\sum_{i=1}^{2} \int {\rm d}^3x\, \rho_i(\mathbf{x})\left[\ln\left(\rho_i(\mathbf{x})\Lambda^3\right) - 1 - \beta\mu_i\right]. \tag{7}$$

In the above-mentioned equation, Λ is the thermal wavelength and μ_i is the chemical potential of the ith species. For a symmetric mixture under equimolarity, the two chemical potentials must be equal. According to the DFT variational principle, the absolute minimum of Eq. (6) is the actual grand potential of the system, whereas the fields providing the minimum value of Ω are the density fields at equilibrium.

In the following Secs. II B–II F, the predictive content of our theory will be illustrated in the case $\xi = 3$, where many simulation results are available from Ref. 46.

B. Homogeneous fluid

For the homogeneous fluid mixture with N_1 type-1 particles and $N_2 = N - N_1$ type-2 particles, the Helmholtz free energy F obtained from the present DFT is given by the standard mean-field approximation,

$$\frac{\beta F}{V} = \frac{\beta F_{\rm HS}(N_1+N_2)}{V} - \beta\frac{N_1N_2}{V^2}|\widetilde{w}_{12}(0)|, \tag{8}$$

where $F_{\rm HS} = Nf_{\rm HS}(N/V)$ and $|\widetilde{w}_{12}(0)| = 4\pi\varepsilon\xi^3/3$ (from now on, the tilde denotes Fourier transformation). For the case of our interest, $N_1 = N_2 = N/2$, and we denote by $\rho = N/V$ the overall number density. From Eq. (8), the pressure and chemical potentials are obtained as

$$\begin{aligned} \beta P &= \beta P_{\rm HS} - \frac{\pi}{3}\beta\varepsilon\rho^2\xi^3, \\ \beta\mu_1 &= \beta\mu_2 = \beta\mu_{\rm HS} - \frac{2\pi}{3}\beta\varepsilon\rho\xi^3, \end{aligned} \tag{9}$$

with

$$\begin{aligned} \beta P_{\rm HS} &= \rho\frac{1+\eta+\eta^2-\eta^3}{(1-\eta)^3}, \\ \beta\mu_{\rm HS} &= \ln\left(\frac{\rho}{2}\Lambda^3\right) + \frac{3-\eta}{(1-\eta)^3} - 3. \end{aligned} \tag{10}$$

Below the critical temperature, Eqs. (9) are non-monotonic functions of the density, and the liquid–vapor coexistence curve is obtained as usual by equating the pressure and chemical potentials of the two phases.

In order for the homogeneous fluid to be stable (or, at least, metastable against some other phase), any departure of the densities from $\rho/2$ must result in an increase of Eq. (6). A necessary condition for stability is then

$$\sum_{i,j=1}^{2} \int {\rm d}^3x \int {\rm d}^3x'\, \left.\frac{\delta^2\beta\Omega}{\delta\rho_i(\mathbf{x})\delta\rho_j(\mathbf{x}')}\right|_{\rho_{1,2}=\frac{\rho}{2}} \delta\rho_i(\mathbf{x})\delta\rho_j(\mathbf{x}') > 0, \tag{11}$$

for arbitrary deviations $\delta\rho_1(\mathbf{x})$ and $\delta\rho_2(\mathbf{x})$. To simplify Eq. (11), we look at the matrix

$$C_{i,j}(\mathbf{x}-\mathbf{x}') \equiv -\left.\frac{\delta^2\beta\Omega}{\delta\rho_i(\mathbf{x})\delta\rho_j(\mathbf{x}')}\right|_{\rho_{1,2}=\frac{\rho}{2}}, \tag{12}$$

whose Fourier transform reads as

$$\widetilde{C}_{i,j}(k) = -\frac{2\delta_{i,j}}{\rho} - \left[2\beta f'_{\rm HS}(\rho) + \rho\beta f''_{\rm HS}(\rho)\right] - \beta\widetilde{w}_{i,j}(k), \tag{13}$$

with

$$\widetilde{w}_{12}(k) = \widetilde{w}_{21}(k) = -4\pi\varepsilon\frac{\sin(k\xi) - k\xi\cos(k\xi)}{k^3}. \tag{14}$$

The inequality (11) is tantamount to requiring that

$$\widetilde{C}_{11}(k) < 0 \quad \text{and} \quad \det\left[\widetilde{C}_{i,j}(k)\right] > 0, \tag{15}$$

for all k. While the first condition is always met, given that

$$\widetilde{C}_{11}(k) = -\frac{2}{\rho}\frac{1+5\eta^2-4\eta^3+\eta^4}{(1-\eta)^4} < 0, \tag{16}$$

the second one is more tricky, and we defer to Appendix A for a thorough discussion of it.

It turns out that the homogeneous fluid can lose stability in two ways: either by developing long-wavelength density fluctuations that give rise to the aforementioned liquid–vapor phase separation ("spinodal instability") or by the onset of inhomogeneities modulated with a wavelength of $2\pi/k_0 \simeq 1.09\xi$, where k_0 is the wave vector at which $\widetilde{w}_{12}(k)$ takes its maximum value. As illustrated in Fig. 1, these instabilities occur at specific loci in the ρ–T plane, respectively, the spinodal line [see Eq. (A7)] and the λ-line [Eq. (A8)]. We anticipate that the spinodal line is well correlated with the liquid–vapor binodal curve obtained from the simulation,[46] while the λ-line marks the upcoming instability of the homogeneous fluid against the formation of stripes of width $\approx\xi/2$.

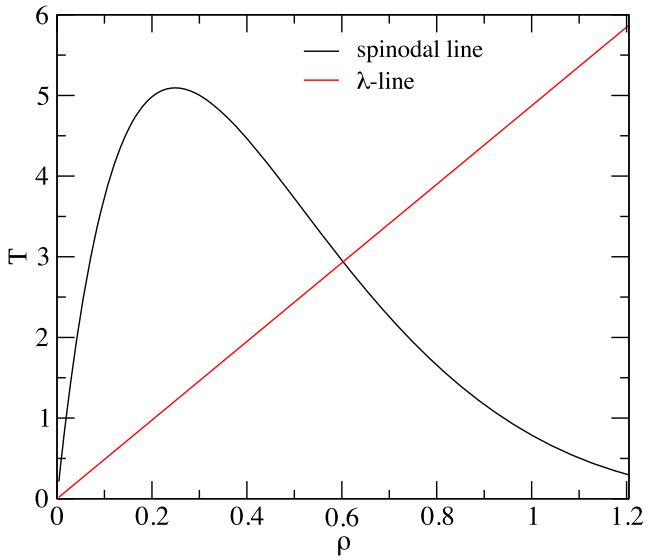

FIG. 1. DFT spinodal line and λ-line for $\xi = 3$ ($\gamma = 2$). Upon cooling the system at constant density, the locus that is encountered first is the one establishing the nature of the instability experienced by the fluid at the given density. For this specific value of ξ, the crossover between the two regimes falls at $\rho \simeq 0.61$.

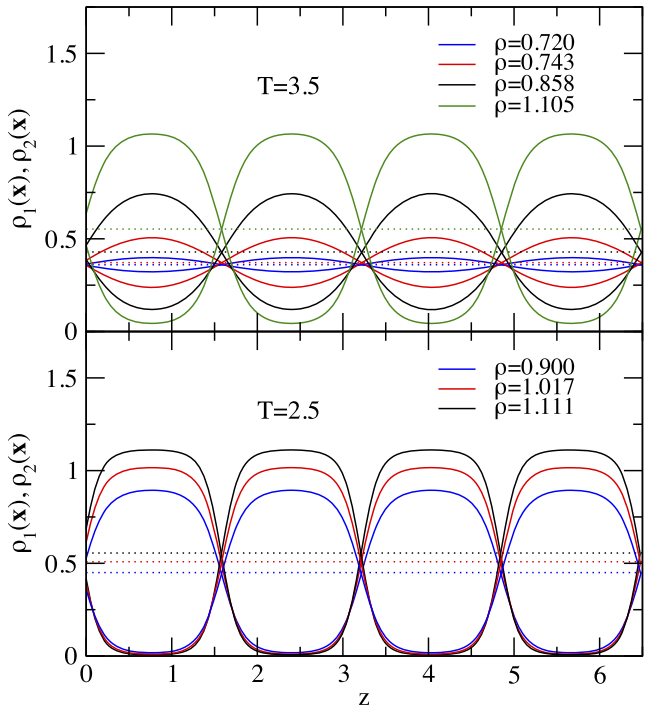

FIG. 2. Density profiles $\rho_1(\mathbf{x})$ and $\rho_2(\mathbf{x})$ at $T = 3.5$ (top) and $T = 2.5$ (bottom) for $\xi = 3$ and several densities reported in the legend, plotted as a function of the coordinate z along the direction of the modulation. Each horizontal dotted line represents the average density $\rho/2$ of both species. Notice how, far away from the λ-line, the density profile clearly differs from a sinusoidal wave and alternates domains almost entirely filled by particles of one species only.

It is worth noting that the study of stability carried out here corresponds to one of the cases described in Ref. 41, although in that paper, the stability analysis was not supplemented with the determination of the phase diagram of the mixture.

C. Numerical minimization

Turning to inhomogeneous phases, a thorough assessment of the theory, which avoids specifying in advance the nature of the inhomogeneity exhibited by the mixture at high density, relies on the numerical minimization of the grand-potential functional. We have accomplished this task using the same algorithm adopted in previous investigations[35,48] and described there in full detail. It turns out that when one enters the region lying to the right of the λ-line in Fig. 1, by either increasing the density or lowering the temperature, phases with a non-uniform density profile become stable. We have verified that minimization runs starting from different trial density profiles always yield stripe-like phases, such that $\rho_i(\mathbf{x})$ varies only along one direction, hence representing a plane density wave.

As illustrated in Fig. 2, for states close below the λ-line, the density profile resembles a sine-like wave superimposed on a uniform background (see, e.g., blue, red, and black lines in the top panel). However, as one plunges more deeply inside the non-homogeneous region (bottom panel), the shape changes markedly, featuring sharp interfaces between regions almost entirely occupied by particles of one species only. The wavelength of the density profile is strongly correlated with $2\pi/k_0 \simeq 1.09\xi = 3.27$: for sine-like modulations, the agreement is to within two significant figures and shows very small deviations even in the sharp-interface limit, where it approximately amounts to 3.26. Figure 2 also indicates that $\rho(\mathbf{x}) = \rho_1(\mathbf{x}) + \rho_2(\mathbf{x})$ deviates very little from the average density ρ. This difference is plotted in Fig. 3 for $T = 5$. Clearly, $\rho(\mathbf{x})$ is not strictly constant except

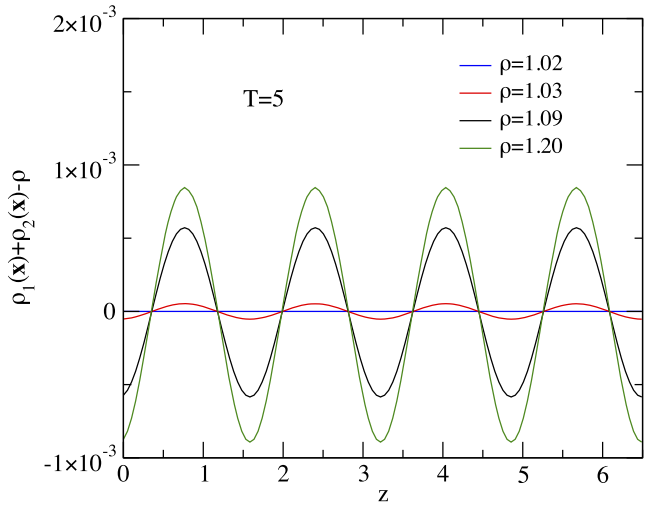

FIG. 3. Deviations of the overall density profile from the average density at $T = 5$ and several ρ values displayed in the legend for $\xi = 3$. Notice the order of magnitude change with respect to the oscillations of the individual density profiles in Fig. 2.

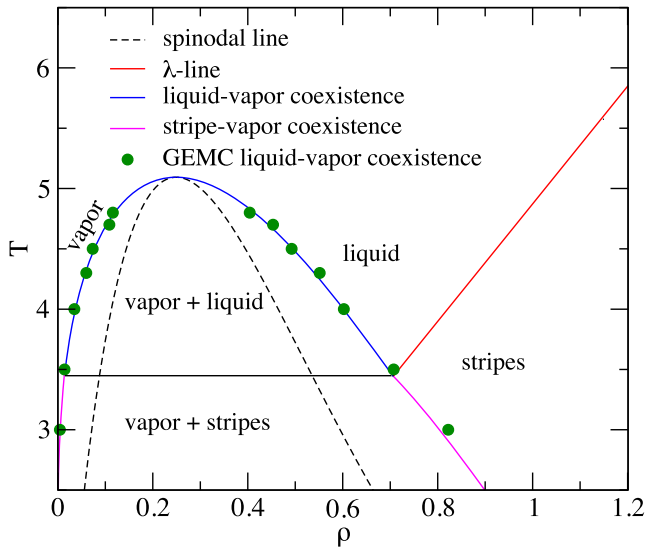

FIG. 4. DFT phase diagram for $\xi = 3$. The green circles are GEMC results from Ref. 46. The critical-point coordinates are $\rho_c = 0.26$, $T_c = 4.89$, as estimated from MC data, while being $\rho_c = 0.249$, $T_c = 5.094$ according to our DFT.

on the λ-line, but its oscillations are much smaller than those of the individual density profiles $\rho_i(\mathbf{x})$.

As the λ-line is approached from within the non-homogeneous region, the amplitude of the density modulation becomes smaller and smaller until it vanishes continuously on the λ-line itself, where the stripe phase merges with the homogeneous fluid. We are then in the presence of a second-order phase transition. This marks an important difference with respect to the phase behavior of $Q^{\pm}$ fluids,[49] where the λ-line has the same shape as found here, but the transition to the inhomogeneous phase—a cluster crystal in that case—is first-order.

Figure 4 displays the phase diagram predicted by the present mean-field DFT approach for $\xi = 3$. The estimated liquid–vapor coexistence is in very good agreement with the Gibbs Ensemble Monte Carlo (GEMC) data points from Ref. 46, reported as circles in the figure. The λ-line meets the liquid–vapor coexistence curve at a critical endpoint. Above the endpoint temperature, the transition from the homogeneous to the striped fluid is second-order. Below the endpoint temperature, the stripe phase coexists with the vapor phase. This phase diagram is akin to one of the three sub-classes exhibited at equimolar conditions by another symmetric mixture, which differs from the one considered here in that attractive interactions also act between particles of the same species and are actually stronger than those between particles of different species.[50,51] However, in that case, the model does not exhibit inhomogeneous phases, and the transition related to the λ-line is rather of the mixing-demixing type.

D. Landau approximation

The evidence provided by numerical minimization is supported near the λ-line (but outside the liquid–vapor coexistence region) by an analytic treatment based on the Landau expansion of the free energy in powers of the amplitude $\mathscr{A}$ of the density modulation, along the same lines pursued in Ref. 52. Let us make the following variational *ansatz* for the density profile:

$$\begin{aligned}\rho_1(\mathbf{x}) &= \frac{\rho}{2}\left[1 + \mathscr{A}\sin(\bar{k}z)\right],\\ \rho_2(\mathbf{x}) &= \frac{\rho}{2}\left[1 - \mathscr{A}\sin(\bar{k}z)\right],\end{aligned} \tag{17}$$

where $\bar{k}$ determines the period of the density modulation. Clearly, Eq. (17) implies $\rho_1(\mathbf{x}) + \rho_2(\mathbf{x}) = \rho$ everywhere, which, albeit not strictly true, is still a sensible approximation, as discussed earlier. We rewrite the Helmholtz free energy $F = F^{\mathrm{id}} + F^{\mathrm{exc}}$ in Eq. (6) as

$$\begin{aligned}\frac{\beta F}{V} &= \frac{1}{v}\sum_{i=1}^{2}\int_v \mathrm{d}^3x\,\rho_i(\mathbf{x})\left[\ln\left(\rho_i(\mathbf{x})\Lambda^3\right) - 1\right]\\ &+ \frac{\beta}{v}\int_v \mathrm{d}^3x\,\left(\rho_1(\mathbf{x}) + \rho_2(\mathbf{x})\right) f_{\mathrm{HS}}\left(\rho_1(\mathbf{x}) + \rho_2(\mathbf{x})\right)\\ &+ \frac{\beta}{v^2}\sum_{\mathbf{k}}\widetilde{\rho}_{1,\mathbf{k}}\widetilde{\rho}_{2,-\mathbf{k}}\,\widetilde{w}_{12}(\mathbf{k}),\end{aligned} \tag{18}$$

where v is the volume of the primitive cell, and the interaction term has been written in Fourier space. By inserting Eq. (17) into Eq. (18), we obtain

$$\frac{\beta F}{V} = \rho\ln\left(\frac{\rho}{2}\Lambda^3\right) - \rho + \rho\beta f_{\mathrm{HS}}(\rho) - \frac{\pi}{3}\beta\varepsilon\rho^2\xi^3 + \frac{\Delta(\beta F)}{V}, \tag{19}$$

with

$$\begin{aligned}\frac{\Delta(\beta F)}{V} &= \frac{\rho}{4\pi}\int_0^{2\pi}\mathrm{d}t\,\left[(1+\mathscr{A}\sin t)\ln(1+\mathscr{A}\sin t)\right.\\ &\left.+\,(1-\mathscr{A}\sin t)\ln(1-\mathscr{A}\sin t)\right] - \frac{1}{8}\widetilde{w}_{12}(\bar{k})\beta\rho^2\mathscr{A}^2.\end{aligned} \tag{20}$$

The first four terms on the right-hand side of Eq. (19) are just the mean-field free energy of the homogeneous fluid mixture, whereas $\Delta(\beta F)/V$ describes the effect of the density modulation and vanishes for $\mathscr{A} = 0$. We note that, within the present approximation, the excess hard-sphere free energy does not contribute to that term. By minimizing Eq. (20) with respect to $\bar{k}$, one finds immediately that $\bar{k}$ has to coincide with the wave vector k_0 at which $\widetilde{w}_{12}(k)$ assumes its maximum. We then get

$$\begin{aligned}\frac{\Delta(\beta F)}{V} &= \frac{\rho}{4\pi}\int_0^{2\pi}\mathrm{d}t\,\left[(1+\mathscr{A}\sin t)\ln(1+\mathscr{A}\sin t)\right.\\ &\left.+\,(1-\mathscr{A}\sin t)\ln(1-\mathscr{A}\sin t)\right] - \frac{\pi}{6}|g(x_0)|\beta\varepsilon\rho^2\xi^3\mathscr{A}^2,\end{aligned} \tag{21}$$

where $g(x_0) \simeq -0.086\,17$ is the minimum of the function $g(x)$ defined in Eq. (A5). The amplitude $\mathscr{A}$ is determined by minimizing Eq. (21).

In the neighborhood of the λ-line, we expect $\mathscr{A}$ to be small so that the integrand can be expanded in powers of $\mathscr{A}$ to give

$$(1+\mathscr{A}\sin t)\ln(1+\mathscr{A}\sin t)+(1-\mathscr{A}\sin t)\ln(1-\mathscr{A}\sin t)$$
$$=\mathscr{A}^2\sin^2 t+\frac{\mathscr{A}^4}{6}\sin^4 t+\cdots. \tag{22}$$

Upon plugging Eq. (22) into Eq. (21) and performing the integration over t, we obtain

$$\frac{\Delta(\beta F)}{V}=\frac{\rho}{4}\alpha\mathscr{A}^2+\frac{\rho}{32}\mathscr{A}^4, \tag{23}$$

with

$$\alpha=1-\frac{2}{3}\pi|g(x_0)|\beta\varepsilon\rho\xi^3=1-4\left(\frac{\xi}{\sigma}\right)^3|g(x_0)|\beta\varepsilon\eta. \tag{24}$$

By comparing Eq. (24) with Eq. (A8), we see that α changes from positive to negative as one crosses the λ-line from left to right in Fig. 1. The minimization of Eq. (23) then follows closely the behavior of the Landau free energy in the Ising model: for $\alpha>0$, the minimum falls at $\mathscr{A}=0$, $\Delta(\beta F)=0$, whereas for $\alpha<0$, it is found at

$$\mathscr{A}=2|\alpha|^{1/2},\quad \frac{\Delta(\beta F)}{V}=-\frac{\rho}{2}\alpha^2, \tag{25}$$

so that the free energy of the striped fluid is indeed lower than that of the homogeneous fluid.

Suppose that the λ-line is approached at a constant temperature from within the non-homogeneous region. Since α vanishes on the λ-line, T can be expressed in terms of the density ρ_λ on the λ-line as [see Eq. (A8)]

$$\frac{k_BT}{\varepsilon}=\frac{2}{3}\pi|g(x_0)|\rho_\lambda\xi^3. \tag{26}$$

By substituting Eq. (26) into Eq. (24), the expression of $\mathscr{A}$ in Eq. (25) becomes

$$\mathscr{A}=2\left(\frac{\rho-\rho_\lambda}{\rho_\lambda}\right)^{1/2}. \tag{27}$$

Within the analytic parametrization of the density profile in Eq. (17), this behavior only holds close to the λ-line, where the expansion (22) is justified. Indeed, the use of Eq. (27) in Eq. (17) for states far away from the λ-line might even lead to unphysically negative density values. We have actually verified that for $T\approx 3$ and densities larger than $\approx$1.2, the free energy of a fluid with sharply defined stripes is slightly lower than that of a sine-wave, in line with the indication coming from numerical minimization (see more in Sec. II E).

The above-mentioned considerations are illustrated in Fig. 5, where the square of the amplitude of the density modulation obtained from the numerical minimization of (6) is plotted against the distance $\rho-\rho_\lambda$ from the λ-line at two temperatures and compared with the prediction of the Landau approach given by Eq. (27), as well as with the result of the minimization of Eq. (21) without performing the expansion in powers of $\mathscr{A}$. As the λ-line is approached, $\mathscr{A}^2$ displays the linear behavior predicted by Eq. (27), although, on increasing $\rho-\rho_\lambda$, deviations from linearity appear soon.

In principle, the analytic picture just illustrated may still be compatible with a first-order transition at high density between the homogeneous fluid and the striped fluid, as found for a different system in Ref. 52. However, this alternative scenario does not apply here because, at a temperature higher than those at which this hypothetical first-order transition would take place, the λ-line hits the high-density branch of the liquid–vapor coexistence curve. Below that temperature, the phase equilibrium involves the striped fluid at high density and the vapor phase at low density, and the corresponding coexistence region supersedes other possible transitions between the striped fluid and the liquid phase.

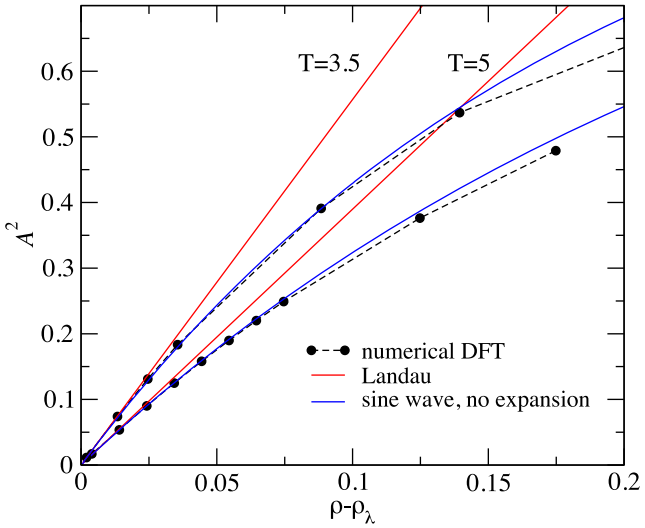

FIG. 5. $\mathscr{A}^2$ vs $\rho-\rho_\lambda$ at $T=3.5$ and $T=5$, for $\xi=3$. The figure shows the predictions based on the fully numerical minimization of Eq. (6) with no ansatz on the density profile, on the numerical minimization with the sine-like parametrization of the density profile [Eq. (21)], and on Landau theory [Eq. (25)].

E. Well within the stripe region

As noted in Sec. II C, well within the region where the stripes are stable (bounded above by the λ-line), a good approximation is to view the striped fluid as a sequence of layers hosting particles of one species only, i.e., 1 and 2 in alternating order. In the following, we show that this modelization allows an analytic expression for the Helmholtz free energy of the striped fluid.

Let us consider an elementary model of striped mixture where the system volume $V=L^3$ is divided into $2M$ horizontal layers B_k (the stripes) of width $\Delta=L/(2M)$ in the z direction, which are alternately populated with type-1 and type-2 spheres,

$$\rho_1(\mathbf{x})=\begin{cases}\rho, & \text{if } \mathbf{x}\in B_k \text{ with } k \text{ odd},\\ 0, & \text{otherwise},\end{cases}$$
$$\rho_2(\mathbf{x})=\begin{cases}\rho, & \text{if } \mathbf{x}\in B_k \text{ with } k \text{ even},\\ 0, & \text{otherwise},\end{cases} \tag{28}$$

where ρ is the overall system density and periodic boundary conditions are implied. In the spirit of Landau's theory, we compare the

free energy of (28) with that of a homogeneous fluid of the same density and temperature. By a trivial calculation, the difference in F^{id}/V between the striped fluid and the homogeneous fluid is $k_BT\rho \ln 2$. While F_{rep} is the same for the two fluids, the calculation of F_{attr}/V yields $-(\pi/3)\xi^3\varepsilon\rho^2$ for the homogeneous fluid and

$$\frac{F_{attr}}{V} = -\frac{\varepsilon\rho^2}{2\Delta}\int_0^{\Delta} dz\, \mathcal{V}(z), \tag{29}$$

for the striped fluid, where $\mathcal{V}(z)$ is the volume that the sphere of radius ξ and center $\mathbf{x} = (0, 0, z) \in B_1$ has in common with one or more stripes B_k with k even.

The integral in Eq. (29) must be performed differently for various intervals of the stripe thickness Δ. This calculation is carried out in Appendix B. In Fig. 6, the ensuing difference in F_{attr}/V between the striped and the homogeneous fluid is plotted as a function of Δ for a few values of ξ. We see that the free-energy gap is minimum and negative for a value of Δ slightly larger than $\xi/2$. This Δ sets the preferred width of the stripes. Calling y the quantity $\Delta F_{attr}/(\varepsilon\rho^2\sigma^3 V)$ plotted in Fig. 6 and $y_{min} < 0$ its minimum value, we conclude that the striped fluid overcomes in stability the homogeneous fluid when

$$\frac{k_BT}{\varepsilon} < \frac{|y_{min}|}{\ln 2}\rho\sigma^3, \tag{30}$$

with, e.g., $|y_{min}|/\ln 2 \simeq 2.85$ for $\xi = 3$ and 6.75 for $\xi = 4$. Upon comparing these values with the slope of the λ-line in (A8), we see that the locus where the striped fluid (28) first overcomes in stability the homogeneous fluid lies below the λ-line, i.e., within the ρ–T region where the homogeneous fluid is unstable. This means that the phase superseding the homogeneous fluid just beyond the λ-line cannot be the one in Eq. (28). This outcome is actually expected: a modelization in which stripes have sharp boundaries cannot hold everywhere in the unstable region since (as shown in Sec. II C) close to the λ-line, the striped fluid of lowest free energy is characterized by a smooth periodic modulation of the density.

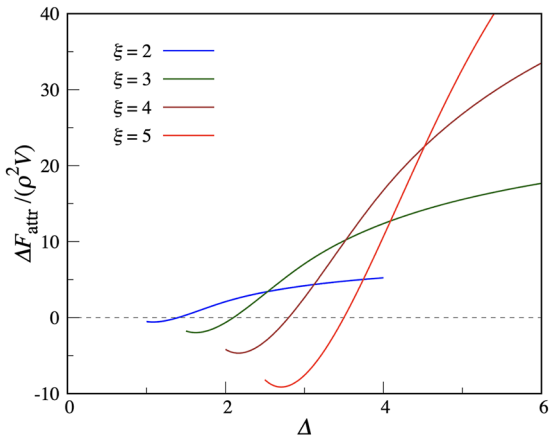

FIG. 6. Difference in the reduced value of F_{attr} between the striped fluid and the homogeneous fluid for a number of ξ values and $\Delta \geq \xi/2$.

F. Freezing

At sufficiently high density, freezing is expected to occur because of the hard-sphere contribution to the free energy of the mixture. Moreover, since the λ-line intersects the solid–fluid coexistence region of hard spheres, freezing will occur both in the absence and in the presence of stripe-like density modulations. In this respect, the phase diagram displayed in Fig. 4 is incomplete because it does not take freezing into account. On the other hand, the local-density approximation (LDA) adopted for the hard-sphere term in (6) is intrinsically unable to describe freezing on the atomic scale. A way to overcome this limitation consists in going beyond LDA, for instance, by employing in the hard-sphere term the weighted-density approximation or the fundamental-measure theory.[53–56] Here, we have considered a rougher and, admittedly, somewhat *ad hoc* approximation to include freezing into the picture, inspired by Eq. (19). According to that expression, which stems from the ansatz in Eq. (17) for the density profile, the contribution $\Delta(\beta F)$ to the free energy due to the density modulation does not contain the hard-sphere term. The present approximation then consists in keeping $\Delta(\beta F)$ unchanged, irrespective of whether the system is fluid or solid, and in replacing the excess free energy per particle of the hard-sphere fluid $f_{HS}(\rho)$ with that of the hard-sphere crystal $f_{HS}^{crystal}(\rho)$. For the latter, we have followed Ref. 57 and adopted the expression deriving from the Hall equation of state.[58] Clearly, in doing so, one assumes that, aside from other approximations, the crystal structure of the system is the same as that of the hard-sphere crystal (i.e., fcc).

A conceptually identical approximation may also be considered in the case where the analytic parametrization of the density profile is not adopted and the numerical minimization of Eq. (6) is taken instead. In that case, we still assume that the attraction-dependent contribution F_{attr} to Eq. (6) is the same for both phases and replace the hard-sphere free energy of the fluid with the hard-sphere free energy of the crystal.

The ensuing phase diagram, inclusive of the crystal phase, is displayed in Fig. 7. In the same figure, we report as full squares some points on the melting and freezing lines taken from Ref. 46. The green lines refer to the analytic parametrization of the density profile, whereas the open squares refer to the unconstrained minimization. In both cases, most of the stripe region is predicted to be in the crystal phase. Below the critical endpoint, a triple point is present, where the vapor, the striped fluid, and the striped crystal coexist.

At low temperatures, the unconstrained minimization deviates appreciably from the analytic parametrization. Indeed, as observed earlier, the latter approximation becomes inaccurate in this regime. According to unconstrained minimization, solid–fluid coexistence takes place at lower densities. As a result, the triple-point is located at a higher temperature: according to the analytic ansatz, the triple temperature falls at $T = 2.48$, whereas unconstrained minimization locates it somewhere near $T = 3$. This is in agreement with the simulation estimate, although we point out that, because of the approximate character of the recipe employed to include freezing, we have failed to obtain solid–fluid coexistence at $T = 3$ within the unconstrained minimization procedure.

As ξ is progressively decreased, no topological change will occur in the phase diagram of Fig. 7, since in both the fluid and

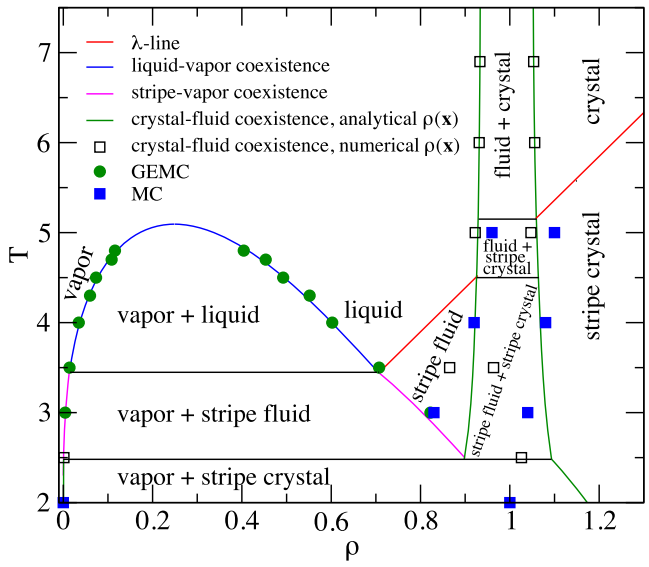

FIG. 7. DFT phase diagram for $\xi = 3$, including the solid phases. The green circles and blue squares, respectively, indicate GEMC liquid–vapor coexistence points and MC estimates of the freezing and melting points.[46]

solid free energies, the values of T and ξ exclusively enter through the combination $k_B T/\xi^3$. This is both an effect of the approximation considered for the solid and an intrinsic limitation of the mean-field treatment of the interaction. However, the same does not hold for the actual system where, upon progressively reducing ξ, the λ-line will eventually end up buried in the solid–fluid and bulk-solid regions, with the result that stripes only appear in the solid phase. Therefore, for small enough values of ξ, the predictions of the theory deviate from simulation. Based on our previous work,[46] the agreement is expected to be good for $\xi = 4$ or larger, whereas for $\xi = 3$, stripes are found only in the solid.

III. SIMULATION

A. General remarks

We address in Monte Carlo (MC) simulations two complementary questions concerning the formation and stability of stripes in our mixture. On one side, the theory presented in Sec. II gives a key to understand the origin of stripes in the liquid phase of the mixture. With the stratagem discussed in Sec. II F, stripes are also predicted to occur in the solid phase. In this case, the transition between the solids with and without the stripes is continuous. However, this is simply the consequence of introducing the solid phase *a posteriori* in a thermodynamically inconsistent way: if we aim to monitor the actual structure and composition of the dense mixture as a function of density and temperature (i.e., beyond the mean-field or any other more sophisticated theory) we cannot manage without numerical simulation.

As for the second question, MC simulations have already been employed in Ref. 46 to compute the liquid and vapor coexistence densities, to estimate the location of the solid–liquid transition for $\gamma = 2$, and to check, in selected cases, the results of total-energy calculations at $T = 0$. In the present study, we use simulation to probe the existence of stripes for $\gamma \leq 1$ since we suspect—by the argument given in Sec. I—that stripes occur in the solid for any γ, no matter how small. In this respect, even an analysis of the dilute system at low temperatures can inform us of the existence of stripes in the solid since, in this case, they will also be seen in the (solid-like) droplet coexistent with vapor. Finally, we also wish to know how stripe order decays with temperature since stripes may either break up abruptly or be disrupted progressively.

B. Method

We carry out canonical Monte Carlo (MC) simulations of samples consisting of a few thousand particles enclosed in a cuboidal box with periodic boundary conditions. After equilibration, we typically generate 10^5–10^6 MC cycles in the bulk liquid or solid, one cycle corresponding to N elementary moves (i.e., displacements of one particle at a time). In the liquid–vapor region, about 5×10^6 MC cycles are needed to bring the system to equilibrium, and as many cycles are needed to obtain accurate statistical averages. To speed up relaxation to equilibrium, we implement swapping moves, where the positions of two randomly chosen unlike particles are interchanged. All moves are accepted according to the Metropolis criterion. It is worth emphasizing that swapping moves are extremely effective in our system: irrespective of the composition set in the initial configuration, the spatial distribution of types evolves to a stationary (equilibrium) distribution in no more than 10^4–10^5 cycles.

Liquid–vapor equilibria are determined by GEMC simulations[59] using 1728 particles that are initially distributed evenly between two boxes of equal volume. We typically carry out runs of 10^6 cycles, where one cycle corresponds to (an average of) N displacement moves plus one volume exchange plus a few hundred particle exchanges (i.e., swaps of particles in different boxes) plus a few dozen swapping moves.

As in Ref. 46, the amount of crystalline order in a given configuration of the system is assessed by computing the Steinhardt bond-angle parameters q_4 and q_6 of every particle.[60–62] Both quantities are nearly zero for a particle having a liquid-like environment, whereas they are significantly non-zero for a solid-like particle. In particular, the values of q_4 and q_6 as averaged over all particles ($\bar{q}_4$ and $\bar{q}_6$) can be used to distinguish a liquid-like from a solid-like droplet in vapor. When combined with visual inspection of the system, the density evolution of the mean Steinhardt parameters gives an effective method to approximately locate the melting point.

We also use another indicator of the overall structure of the mixture, namely, the pair entropy per particle s_2. For a fluid mixture of two species, the latter is given by[63]

$$s_2 = -\frac{k_B}{2}\sum_{i,j=1}^{2} \chi_i \chi_j \rho \int \mathrm{d}^3 r \,[g_{i,j}(r) \ln g_{i,j}(r) - g_{i,j}(r) + 1], \qquad (31)$$

where χ_i is the concentration of the ith species (here equal to 0.5 for both particle types) and $g_{i,j}(r)$ are radial distribution functions. While in a crystal, the definition of s_2 is different,[64] the same formula (31) is employed here also for a solid mixture, which generally results in a large negative s_2 value. Conversely, $|s_2| \approx k_B$ in a fluid configuration.

Finally, the presence of stripes in the mixture, be it solid or liquid, is ascertained by introducing a convenient order parameter O. Let us first consider, for the sake of clarity, a crystalline (fcc or hcp) configuration. For simplicity, hereafter we only foresee the possibility of planar stripes made up of $n_s = 1$ or 2 lattice planes, lying perpendicularly to a high-symmetry z direction [001], [011], or [111] for fcc, whereas in the hcp case, stripes are taken to consist of (0001) planes. Now, let us call c_i and z_i the type and z position of the ith particle (with, say, $c_i = 1$ for a type-1 particle and -1 for a type-2 particle). Denoting the z separation between two adjacent horizontal planes of particles by a, we define

$$O = \left\langle \frac{1}{\mathcal{N}} \left| \sum_{j=1}^{N} c_j e^{ikz_j} \right| \right\rangle \quad \text{with} \quad k = \frac{2\pi}{n_s a}, \tag{32}$$

where the normalization constant $\mathcal{N} = N$ for $n_s = 1$ and $N/\sqrt{2}$ for $n_s = 2$. The order parameter (32) recalls the one employed in studies of smectic-A order in liquid crystals, see, e.g., Ref. 65; indeed, smectic layers are nothing but stripes perpendicular to the nematic director.

To follow the thermal evolution of O in a specific solid, we proceed as follows. At a certain low temperature, say $T = 0.3$, the mixture is initially arranged in a crystalline configuration with composition modulated in the z direction and then equilibrated. Next, keeping the density ρ fixed, the temperature is increased in small steps, taking as the initial configuration of the system at a given temperature the last configuration generated at the previous temperature. If, at any moment during the simulation, stripes are still present in the sample and are oriented perpendicularly to z, then O is non-zero; otherwise, O takes a nearly zero value.

With the (somewhat arbitrary) normalization $\mathcal{N} = N$, the order parameter (32) can also be employed for a striped liquid. For O to be an effective indicator of stripe order, (a) the stripes must lie perpendicularly to z, and (b) the value of a should match the mean z difference between two adjacent stripes. In practice, a has to be adjusted during the equilibrium run in such a way that O acquires its maximum value.

C. Results

As mentioned earlier, our first purpose is to determine the lowest value of γ for which stripes are present in the solid phase of the mixture. In addition to that, we wish to investigate how stripe order decays in the solid as the temperature is increased at a fixed density.

We begin by providing evidence of the existence of stripes in the solid for $\gamma = 1$. In our previous study,[46] we concluded that for this value of γ, stripes are absent in the liquid phase. For $T = 1$ (a value well below the critical temperature $T_c \approx 1.48$), we also verified that the liquid–vapor interface undergoes a sequence of geometric transitions with increasing density:[66–68] for relatively low densities, the liquid forms a spherical droplet in equilibrium with the vapor; for higher densities, the shape of the droplet becomes cylindrical or slab-like. The scenario changes when the temperature is reduced to 0.5, as illustrated in the system snapshots reported in Fig. 8. Between $\rho = 0.10$ and $\rho = 0.30$, we observe the same sequence of shapes found at $T = 1$, but spheres are now organized in parallel stripes of alternating type, and the structure of the droplet is more compact. Indeed, for $\rho = 0.10$ [(a), where the droplet is spherical] and $\rho = 0.20$ [(b), where the droplet is cylindrical], we see facets on the droplet surface, whereas for $\rho = 0.30$ (c), the surface of the slab-like droplet is perfectly flat. The mean Steinhardt parameters confirm that, away from the surface, the droplets in (a)–(c) consist of solid-like particles. Therefore, for $T = 0.5$, the mixture for $\gamma = 1$ is below its triple temperature. The existence of stripes in the solid system is evident in panel (d), showing a typical snapshot of the bulk fcc crystal for $\rho = 1.10$.

The observation of a well-ordered stripe pattern for $\gamma = 1$, a value not distant from the ranges typical of colloidal interactions, prompts us to investigate even shorter SW ranges. First, we lower γ from 1 to 0.5. It is known from studies of pure SW systems[69–71] that a progressive shrinking of the attraction range makes the critical temperature smaller and smaller until liquid–vapor coexistence becomes metastable with respect to solid–fluid equilibrium—an event occurring for SW widths shorter than 0.25σ. Since in our model, the SW attraction is only exerted between unlike spheres, the metastability threshold might, in principle, be higher. Therefore, we have first verified that a stable liquid–vapor separation is indeed present for $\gamma = 0.5$. For this range of attraction, we report in Fig. 9 some GEMC data suggesting that the liquid and vapor phases truly separate below a critical temperature of ≈ 0.70. At variance with the case of a wide well ($\gamma = 2$), for $\gamma = 0.5$, the mean-field critical temperature turns out to be appreciably smaller than the true one. This behavior is similar to what occurs in pure SW fluids for narrow wells,[71] even though, in both cases, the situation is bound to reverse in the limit $\gamma \to 0$ when the mean-field approximation used here incorrectly predicts a non-vanishing critical temperature because of the residual attraction inside the repulsive core [see Eq. (5)].

To exclude the possibility that the whole binodal line in Fig. 9 is metastable, we have investigated the behavior of the mean Steinhardt parameters as a function of the density for various temperatures

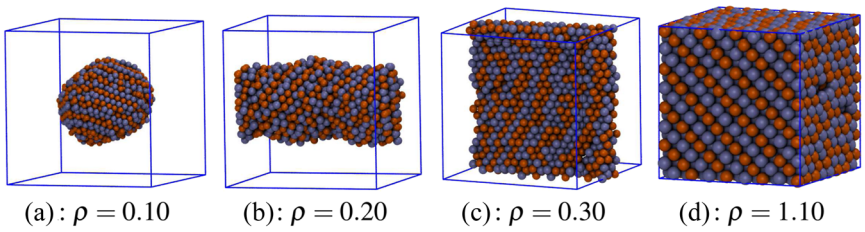

FIG. 8. Typical equilibrium configurations of the mixture with $\gamma = 1$, $T = 0.5$, and a number of densities. (a) $\rho = 0.10$. (b) $\rho = 0.20$. (c) $\rho = 0.30$. (d) $\rho = 1.10$.

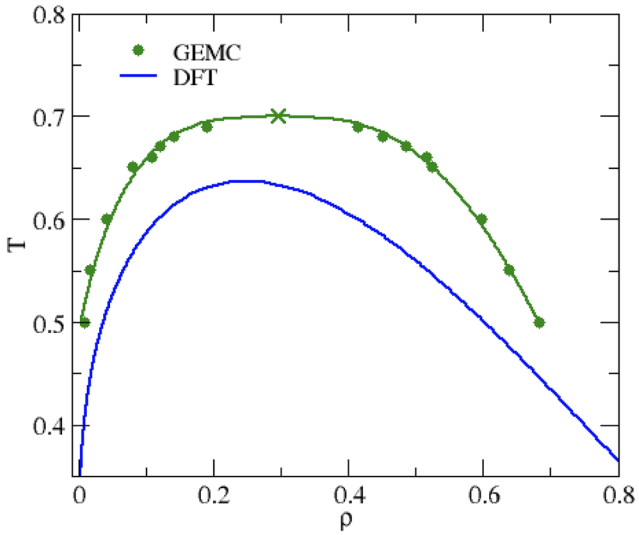

FIG. 9. Liquid–vapor equilibrium in the mixture with $\gamma = 0.5$: GEMC data points (green circles) are compared with the coexistence line derived from DFT (blue line). The GEMC critical-point coordinates are found to be $\rho_c = 0.297$ and $T_c = 0.700$, as obtained by fitting the coexistence data to the scaling law expected for the density difference between the phases and to the law of rectilinear diameters.[59] According to DFT, the coordinates of the critical point are instead $\rho_c = 0.249$ and $T_c = 0.637$.

around 0.5. In practice, starting from the perfect fcc crystal at $\rho = 1.30$, we gradually expand the mixture isothermically, equilibrating it at each step until reaching $\rho = 0.40$. In Fig. 10, left, we show the results obtained for $T = 0.5$ and 0.6. The behavior of $\bar{q}_4$ and $\bar{q}_6$ is similar: starting from the bulk-solid values, these quantities begin to decrease at $\rho \simeq 1.22$, i.e., near the melting density. Then, at $\rho \simeq 0.90$, the behaviors at the two temperatures become different.

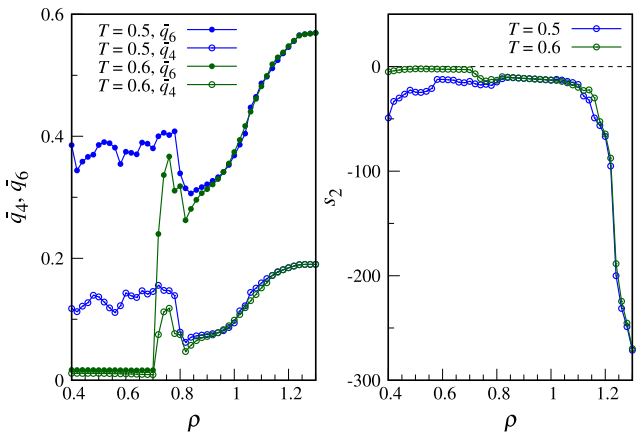

FIG. 10. Mean Steinhardt parameters $\bar{q}_4$ and $\bar{q}_6$ (left) and two-body entropy s_2 (right) for $\gamma = 0.5$, plotted as a function of the density at $T = 0.5$ and 0.6.

For $T = 0.6$, the mean Steinhardt parameters undergo a substantial enhancement near $\rho = 0.75$ (probably in the vicinity of a geometric transition) but eventually decrease again and vanish, together with s_2, at $\rho = 0.70$. Looking at the binodal line in Fig. 9, we argue that the system is a bulk liquid between $\rho \simeq 0.60$ and $\rho \simeq 0.70$. Instead, for $T = 0.5$, $\bar{q}_4$ and $\bar{q}_6$ remain non-zero all the way down to low densities, meaning that part of the system remains solid (this is confirmed by visual inspection of the system at $\rho = 0.40$, revealing a slab-like solid droplet suspended in vapor). In parallel, $|s_2|$ (Fig. 10, right) acquires larger and larger values due to the development of large-distance oscillations in the radial distribution functions. Therefore, we conclude that the triple temperature for $\gamma = 0.5$ falls between 0.5 and 0.6. As for the compositions, we confirm the existence of stripes in the solid for $\gamma = 0.5$. This will be discussed in detail below, in parallel with the case $\gamma = 0.1$.

Let us finally consider the mixture with $\gamma = 0.1$. For this narrow attraction range, we were not able to draw a liquid–vapor coexistence locus by GEMC. However, stripes still exist—see, e.g., the snapshot in Fig. 11(a), corresponding to $\rho = 1.1$ and $T = 0.5$. Here, each stripe consists of a single plane of particles of the same species, with square order within the planes. However, as we see better in Fig. 11(b), particles are fluid-like in a portion of the simulation box corresponding to two missing planes, suggesting that the state point under scrutiny actually falls inside the solid–fluid coexistence region. This conclusion is confirmed by the density evolution of the mean Steinhardt parameters and pair entropy along a few isotherms (see Fig. 12). We see that the initially fcc-ordered system enters the solid–fluid region at $\rho \simeq 1.15$, almost independently of T. As expected, the coexistence region is much wider at $T = 0.3$ than at $T = 0.5$ or 1. We have not explored values of γ smaller than 0.1, but it is reasonable to think that stripes will be present at low temperatures for any positive γ, at least in a range of densities close to the maximum density $\sqrt{2}$.

We now turn to characterize the thermal behavior of stripes in the solid phase of the mixture for $\gamma = 0.1, 0.5$, and 1. We initially set $T = 0.3$ and prepare the mixture in a striped crystalline configuration of high density. Then, we gradually increase the temperature while keeping the density fixed, bringing the sample to equilibrium at each T. As anticipated in Sec. III B, we explore various possibilities for the initial structure of the mixture. Zero-temperature calculations[46] for $\gamma = 0.1$ and 0.5 suggest that, in equilibrium, stripes consist of just one lattice plane ($n_s = 1$); hence, only this case is examined;

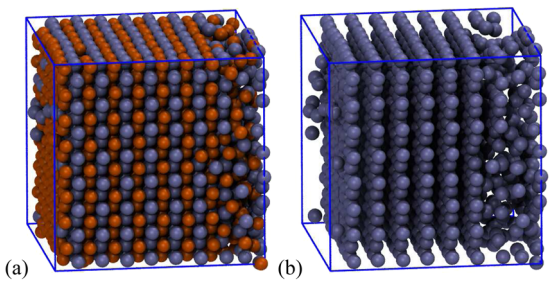

FIG. 11. Typical equilibrium configuration of the mixture with $\gamma = 0.1$, $T = 0.50$, and $\rho = 1.10$ (a). To better highlight the striped nature of the crystal, one species has been hidden in panel (b).

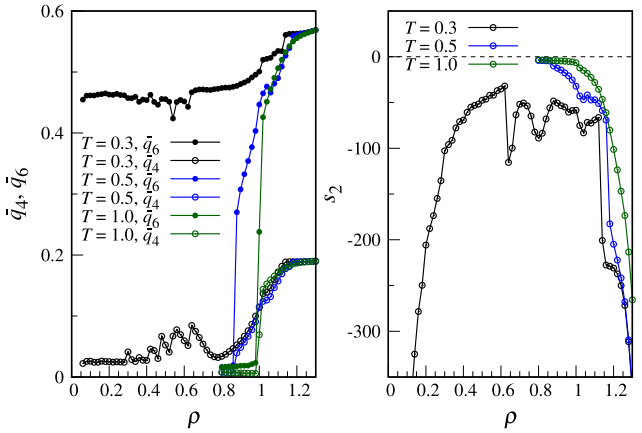

FIG. 12. $\bar{q}_4$ and $\bar{q}_6$ (left) and s_2 (right) for $\gamma = 0.1$, at $T = 0.3, 0.5$, and 1.

for $\gamma = 1$, we instead consider both $n_s = 1$ and $n_s = 2$. Since the two species are mixed at random in the high-temperature solid, an isostructural "transition"—i.e., either a true phase transition or a smooth crossover—should take place upon heating from the striped solid to the compositionally disordered solid. To clarify this issue, we have monitored the T dependence of the order parameter O and the potential energy per particle U/N.

In Fig. 13, we show results for $\gamma = 0.1$ [panels (a) and (c)] and $\gamma = 0.5$ [panels (b) and (d)], with the density fixed at $\rho = 1.3$. For $\gamma = 0.1$, stripes resist thermal fluctuations only in the fcc001 and fcc011 solids, whereas in the fcc111 solid, the initial stripes are re-oriented by the swapping moves, already at the initial temperature $T = 0.3$, along either [001] or [011]; also in the hcp solid, the initial stripes disappear rather quickly. It is worth noting that, due to the very short range of attraction, various striped solids have essentially the same energy, implying an effective thermodynamic degeneracy too. That said, the important message of Fig. 13 is that, for $\gamma = 0.1$, stripe order vanishes near $T \simeq 0.88$ with a seemingly first-order transition (we have verified that the same occurs for $\rho = 1.2$, where O vanishes abruptly at $T = 0.73$). This is to be contrasted with the behavior at $\gamma = 0.5$, where stripes consist of single planes with triangular order: as the solid is heated up, stripe ordering persists up to $T \simeq 1.75$, where it vanishes smoothly. Hence, for $\gamma = 0.5$, we do not see a sharp solid–solid transition but rather a progressive rearrangement of the compositions.

We have verified that the transition from compositional order to disorder is completely reversible, at least when a unique ground state exists for the given crystalline structure—for instance, in the case of $\gamma = 0.5$. For $\gamma = 0.1$, upon gradually cooling a compositionally disordered fcc crystal, the ordered mixture eventually formed contains patches with fcc001 order mixed together with patches with fcc011 order.

A separate case is $\gamma = 1$, which is illustrated in Fig. 14. Here, we report the thermal behavior of O and U/N for two densities, $\rho = 1.1$ [panels (a) and (c)] and $\rho = 1.3$ [panels (b) and (d)]. We consider two distinct patterns of stripes for the initial configuration of the mixture at $T = 0.3$, namely, $n_s = 1$ and $n_s = 2$. At the lower density,

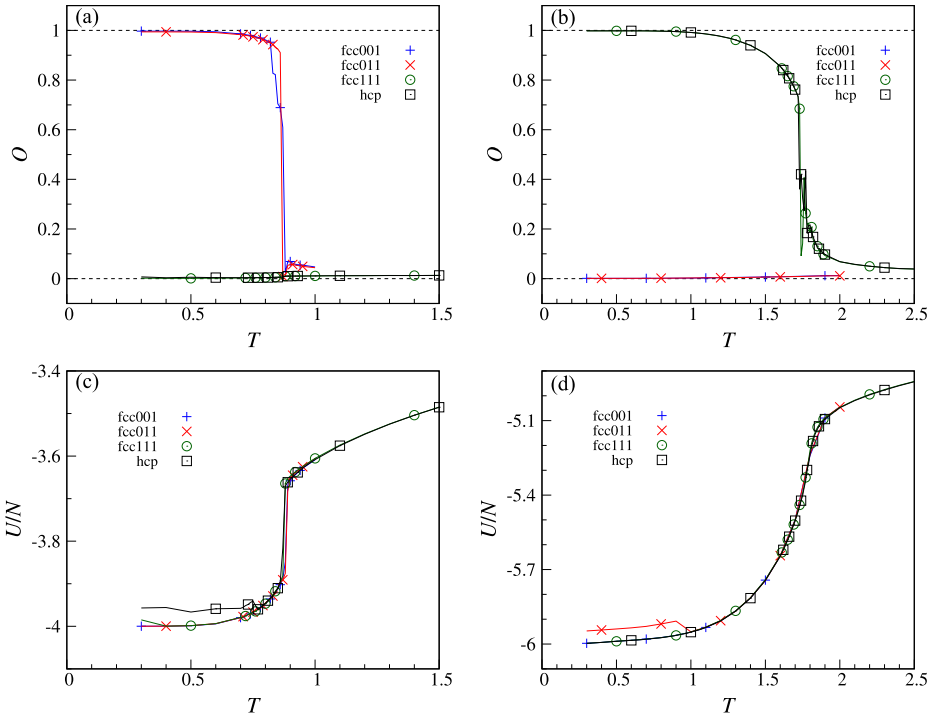

FIG. 13. Order parameter and excess energy per particle for $\gamma = 0.1$ [(a) and (c)] and $\gamma = 0.5$ [(b) and (d)]. The density is $\rho = 1.3$.

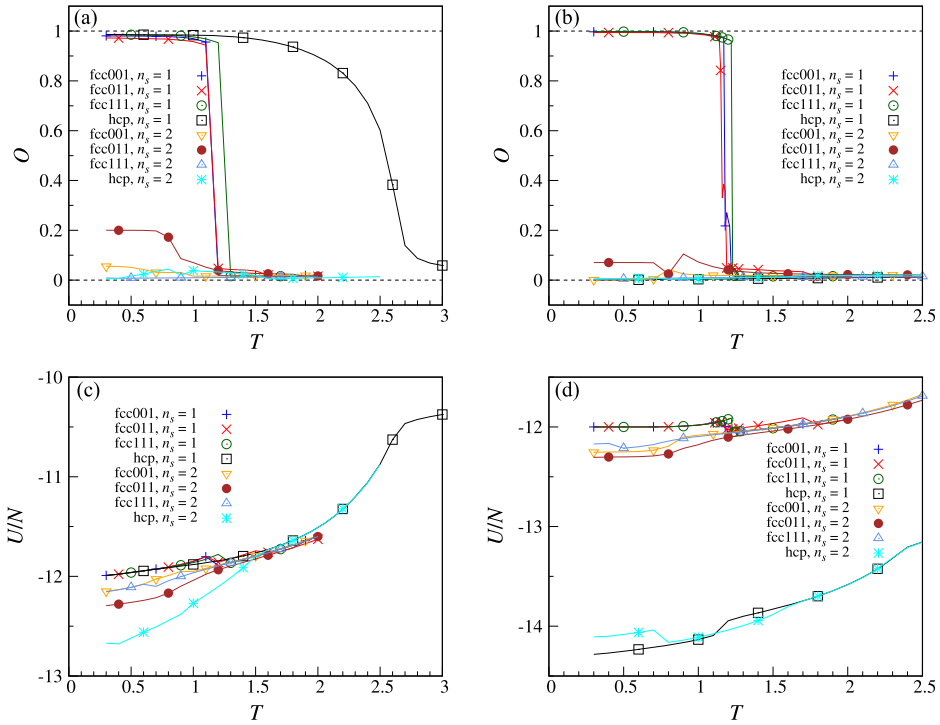

FIG. 14. Order parameter and excess energy per particle for $\gamma = 1$. The density is $\rho = 1.1$ in panels (a) and (c), and $\rho = 1.3$ in panels (b) and (d).

stripes are stable in any of the four structures/orientations considered for $n_s = 1$, and particularly so in the hcp case where stripe order survives till rather high temperatures, $T \simeq 2.5$. However, at low temperatures, the minimum energy (and, presumably, also free energy) value corresponds to hcp with $n_s = 2$, where the initial stripes are washed out by thermal fluctuations already at $T = 0.3$. Indeed, visual inspection of the system at $T = 0.3$ indicates that, in equilibrium, the compositional order preferred at $\rho = 1.1$ is a less regular alternation of single and double (0001) planes filled with particles of the same species. Only at $T \approx 1.6$, a smooth crossover to a striped hcp phase with $n_s = 1$ eventually occurs.

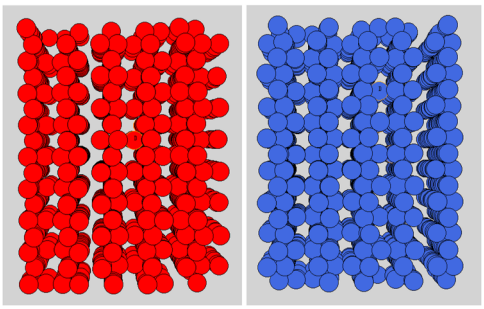

FIG. 15. Snapshot of the typical equilibrium configuration of the mixture with $\gamma = 1$, for $\rho = 1.3$ and $T = 0.3$. In the two panels, type-1 and type-2 particles are hidden in turn, so as to clearly identify the positions of each species of particles.

Moving to $\rho = 1.3$, we see in Fig. 14(d) that the stability of the hcp solid is now much higher than that of any fcc competitor. However, at low temperatures, the stable mixture with $\gamma = 1$ is not a striped solid but something different (see Fig. 15). In this picture, which displays the typical equilibrium configuration of the system at low temperatures, we see that the mixture is still compositionally ordered, but the particles of each species form a (self-dual) regular porous matrix holding in its interstices the particles of the other species. We have not further inquired into the precise disposition of particles in the hcp lattice since we have verified that it slightly depends on the shape of the simulation box, i.e., on the degree of commensuration of the system.

In conclusion, the compositional order exhibited by the mixture with $\gamma = 1$ is not stripe-like. This model falls somehow at the boundary between striped mixtures with $n_s = 1$ and $n_s = 2$. We conclude that the competition between two distinct values of the stripe thickness makes stripe order frustrated for $\gamma = 1$, opening the way to novel ground states where the compositional order is more complex and density-dependent.

IV. CONCLUSIONS

We have investigated a model of binary mixture, originally introduced in Ref. 46, in which condensation is driven by a short-range attraction between unlike particles. To keep it simple, the particles are modeled as hard spheres of the same diameter σ and equal concentration, while the cross attraction is taken to be a SW

potential of range $(1+\gamma)\sigma$. In our previous work, we have shown that at sufficiently low temperatures, the solid phase of the mixture for $\gamma \geq 1$ is stripe-ordered, in that the two species form layers of alternating types, running along a direction. Moreover, stripes also appear in the liquid phase when γ is sufficiently large.

In this paper, we considerably extend the analysis in Ref. 46 by first applying a DFT that accounts well for the behavior of the mixture in the fluid sector of the phase diagram (at least provided that γ is sufficiently large); by an *ad hoc* modification, the solid phase of the mixture can be described too. Specifically, the liquid–vapor equilibrium compares well with simulation results; in further agreement with simulation, the homogeneous fluid becomes unstable at high density against a striped fluid, and the expected phase transition is second-order. Finally, the theory predicts two solid phases, i.e., with and without the stripes, separated by a continuous transition.

We underline that the occurrence of a liquid–vapor transition, in addition to that of inhomogeneous microphases, is a prominent feature of the present model, which makes it particularly interesting and different from the models investigated in Refs. 35 and 48, where instead no liquid–vapor equilibrium occurs.

Next, using Monte Carlo simulations, we have focused on the crystalline phases of the mixture, showing the existence of stripes in the solid for γ as small as 0.1. For this γ, the transition from the striped crystal to one with compositional disorder is sharp, whereas it is a smooth crossover for $\gamma = 0.5$ or 1. In the latter case as illustrated in Fig. 15, the compositional order exhibited by the mixture is actually more complex, an outcome which is imputed to the unresolvable competition between two distinct values of the stripe thickness.

We may easily guess that the observed behavior also occurs at concentrations slightly away from equimolarity. At the same time, we cannot exclude that a larger difference in concentration between the species could lead to other kinds of orderings, such as, e.g., those observed for a different model mixture in Ref. 48, where the species at lower concentrations arranges itself in spherical clusters or cylinders and the species at higher concentrations percolates in the space left available. Moreover, the study carried out in Ref. 41 shows that both the spinodal and the λ-line of the mixture are strongly affected by changes in concentration, so the topology of the phase diagram may change as well. Studies are currently underway to clarify these issues. Moreover, preliminary calculations suggest that many characteristics of the present model could be owned by a whole class of mixtures where the like interactions are short-range repulsive and the cross interactions are generically attractive. In a forthcoming paper, we will provide wide evidence of this universality of behavior. In this respect, we note that stripe patterns have also been observed in equimolar mixtures where both like and unlike interactions feature a repulsive and an attractive term.[43] Similarly as occurs in our mixture for large γ, in that model, the vapor may coexist with liquid, striped-liquid, and striped-solid phases. However, there are also differences insofar as, in the mixture investigated in Ref. 43, the transition between liquid and striped liquid is first-order.

The unexpected variety of emergent behaviors in the basic model considered here can stimulate the search for colloidal mixtures with similar behaviors. In particular, striped mixtures can find immediate application in the development of photonic devices; for this reason, the identification of a simple mechanism for the formation of stripe patterns in binary mixtures can be of considerable technological interest.

ACKNOWLEDGMENTS

D.P. acknowledges support from the Università degli Studi di Milano, Project No. PSR2022_DIP_008-Linea 2. This work has been performed using the computer facilities made available by the PO-FESR 2007–2013 Project MedNETNA (Mediterranean Network for Emerging Nanomaterials).

AUTHOR DECLARATIONS

Conflict of Interest

The authors have no conflicts to disclose.

Author Contributions

Santi Prestipino: Conceptualization (equal); Investigation (equal); Methodology (equal); Supervision (equal); Writing – original draft (equal). **Davide Pini**: Conceptualization (equal); Investigation (equal); Methodology (equal); Supervision (equal); Writing – original draft (equal). **Dino Costa**: Supervision (equal); Writing – review & editing (equal). **Gianpietro Malescio**: Supervision (equal); Writing – review & editing (equal). **Gianmarco Munaò**: Conceptualization (equal); Investigation (equal); Supervision (equal); Writing – review & editing (equal).

DATA AVAILABILITY

The data that support the findings of this study are available from the corresponding author upon reasonable request.

APPENDIX A: ON THE STABILITY OF THE HOMOGENEOUS FLUID

In this appendix, we report calculations relative to the DFT of Sec. II, which, for ease of reading, have not been included in the main text. Specifically, we determine the instability loci of the homogeneous fluid mixture.

Let $\widetilde{c}_{\rm HS}(\rho)$ be the Fourier transform of the direct correlation function of a fluid of hard spheres at density ρ. Within the local-density approximation adopted here for the excess free energy functional $F_{\rm rep} = \int {\rm d}^3x \rho(\mathbf{x}) f_{\rm HS}(\rho(\mathbf{x}))$, $\widetilde{c}_{\rm HS}(\rho)$ does not depend on the wave vector k and is given by

$$\widetilde{c}_{\rm HS}(\rho) = -2\beta f'_{\rm HS}(\rho) - \rho\beta f''_{\rm HS}(\rho) = -\frac{\pi}{3}\sigma^3 \frac{4-\eta}{(1-\eta)^4}. \tag{A1}$$

Then, the elements of the matrix (13) can be written as

$$\begin{aligned} \widetilde{C}_{11}(k) &= \widetilde{C}_{22}(k) = -\frac{2}{\rho} + \widetilde{c}_{\rm HS}(\rho)\,; \\ \widetilde{C}_{12}(k) &= \widetilde{C}_{21}(k) = \widetilde{c}_{\rm HS}(\rho) - \beta\widetilde{w}_{12}(k), \end{aligned} \tag{A2}$$

and the determinant becomes

$$\det\left[\widetilde{C}_{i,j}(k)\right] = \left[\widetilde{C}_{11}(k) + \widetilde{C}_{12}(k)\right]\left[\widetilde{C}_{11}(k) - \widetilde{C}_{12}(k)\right] = \left[-\frac{2}{\rho} + 2\widetilde{c}_{\rm HS}(\rho) - \beta\widetilde{w}_{12}(k)\right]\left[-\frac{2}{\rho} + \beta\widetilde{w}_{12}(k)\right], \quad \text{(A3)}$$

or equivalently,

$$\det\left[\widetilde{C}_{i,j}(k)\right] = 4v_0^2\left[\frac{1}{\eta} - \frac{\widetilde{c}_{\rm HS}(\rho)}{v_0} - 4\left(\frac{\xi}{\sigma}\right)^3\beta\varepsilon g(k\xi)\right] \times \left[\frac{1}{\eta} + 4\left(\frac{\xi}{\sigma}\right)^3\beta\varepsilon g(k\xi)\right]. \quad \text{(A4)}$$

In the above equation, $v_0 = \eta/\rho = \pi\sigma^3/6$ is the hard-sphere volume and

$$g(x) = \frac{3}{x^3}(\sin x - x\cos x) \quad \text{with} \quad g(0) = 1. \quad \text{(A5)}$$

The first factor in Eq. (A4) is akin to minus the Fourier transform of the (mean-field expression of the) direct correlation function of the pure SW fluid, including the ideal-gas contribution, and behaves in the same way. If we fix the density and set $k = 0$, this factor changes sign from positive to negative as T is decreased. Moreover, since $g(x)$ takes its absolute maximum at $x = 0$ [i.e., $\widetilde{w}_{12}(k)$ takes its absolute minimum at $k = 0$], the first wave vector at which the sign changes is indeed $k = 0$, corresponding to a spinodal instability. The spinodal line in the ρ–T plane is then

$$\beta\varepsilon = \frac{1}{4}\left(\frac{\sigma}{\xi}\right)^3\left[\frac{1}{\eta} - \frac{\widetilde{c}_{\rm HS}(\rho)}{v_0}\right], \quad \text{(A6)}$$

or, explicitly,

$$\beta\varepsilon = \left(\frac{\sigma}{\xi}\right)^3\left[\frac{1}{4\eta} + \frac{4-\eta}{2(1-\eta)^4}\right]. \quad \text{(A7)}$$

In turn, the second factor in Eq. (A4) is similar to minus the Fourier transform of the direct correlation function of a fluid of penetrable particles interacting via the repulsive square-shoulder potential $-w_{12}(r)$. This interaction belongs to the class of so-called $Q^{\pm}$ potentials;[49] indeed, the function $g(x)$ changes sign first at $x \simeq 4.4934$ and reaches its absolute minimum at $x_0 \simeq 5.7635$. Since this minimum is negative, the second factor in Eq. (A4) turns from positive to negative as T is decreased at a fixed density. However, the wave vector at which this occurs is now k_0, such that $k_0\xi = x_0$. Therefore, we are in the presence of an instability at $k_0 \neq 0$, corresponding to a λ-line whose equation on the ρ–T plane is given by

$$\frac{k_BT}{\varepsilon} = 4\left(\frac{\xi}{\sigma}\right)^3|g(x_0)|\eta, \quad \text{(A8)}$$

with $|g(x_0)| \simeq 0.086\,17$. This instability locus has the same linear behavior as the λ-line of $Q^{\pm}$ fluids in the random-phase approximation.

Looking at Eq. (A4), when the spinodal line is crossed by decreasing T at constant density, the first factor evaluated at $k = 0$ becomes negative at the spinodal line. Similarly, when the λ-line is crossed by decreasing T, it is the second factor evaluated at $k = k_0$ that becomes negative. On the other hand, since $g(0)$ is positive and $g(x_0)$ is negative, both the second factor evaluated at $k = 0$ and the first factor evaluated at $k = k_0$ are positive. Therefore, as either the spinodal line or the λ-line is crossed, the determinant (A4) turns negative, and the stability condition for the fluid is violated, respectively, at $k = 0$ and $k = k_0$.

Figure 1 displays the spinodal line and the λ-line for $\xi = 3$. The wave vector at which the instability of the homogeneous fluid first occurs at high density is related to the periodicity of the inhomogeneous phase that supersedes it. For the striped phase, this is close to $2\pi/k_0 = 2\pi\xi/x_0 \simeq 3.27$.

APPENDIX B: CALCULATION OF THE INTEGRAL IN EQ. (29)

To evaluate the integral in Eq. (29), we should proceed differently, depending on the stripe thickness Δ. Let us first take $\Delta \geq \xi$. We can make reference to Fig. 16, where we see a projection of the overlapping geometry onto the x–z or y–z plane. The z coordinates of the points A, B, C, and D are $z + \xi, \Delta, 0$, and $z - \xi$, respectively. The sphere of radius ξ and center $\mathbf{x} = (0, 0, z)$ in B_1 (i.e., $0 \leq z \leq \Delta$) can at most intersect two even-numbered layers, namely, B_2 (if $z > \Delta - \xi$) and B_{2M} (if $z < \xi$), lying, respectively, above and below B_1. Each overlapping region has the shape of a one-base spherical segment of height $\overline{\rm AB}$ (top) or $\overline{\rm CD}$ (bottom). Since the volume of a spherical segment of height h, cut out of a sphere of radius R, is $\pi h^2(R - h/3)$, the overlapping volumes turn out to be $\pi(z + \xi - \Delta)^2(\xi - (z + \xi - \Delta)/3)$ (for $\Delta - \xi \leq z \leq \Delta$) and $\pi(\xi - z)^2(\xi - (\xi - z)/3)$ (for $0 \leq z \leq \xi$), respectively. Therefore, we obtain

$$\int_0^{\Delta} {\rm d}z\, \mathscr{V}(z) = \pi\int_{\Delta-\xi}^{\Delta} {\rm d}z\,(z + \xi - \Delta)^2\left(\xi - \frac{z + \xi - \Delta}{3}\right) + \pi\int_0^{\xi} {\rm d}z\,(\xi - z)^2\left(\xi - \frac{\xi - z}{3}\right) = \frac{\pi}{2}\xi^4. \quad \text{(B1)}$$

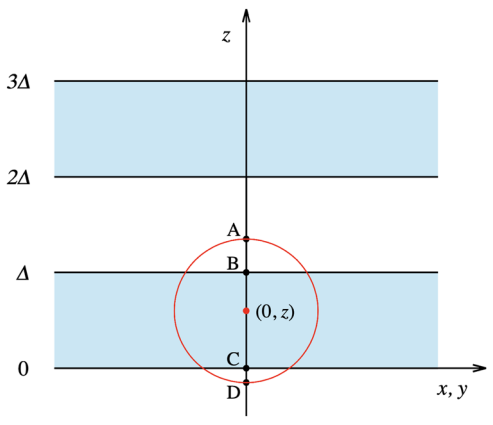

FIG. 16. Geometry of the problem for the case $\xi \leq \Delta$ (see text).

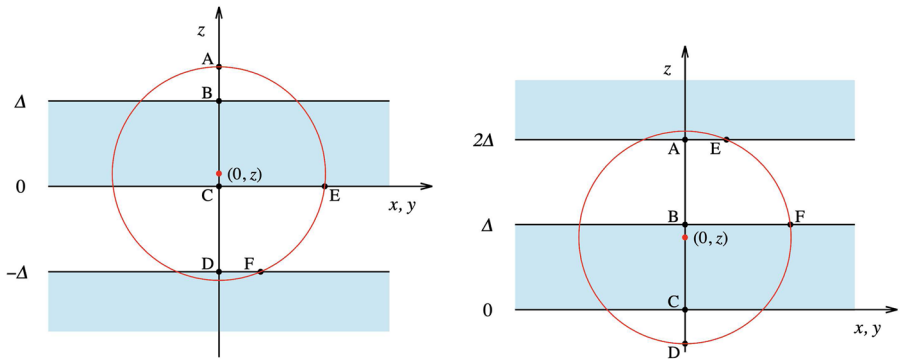

FIG. 17. Geometry of the problem for $\Delta \le \xi < 2\Delta$ (see text) in the two cases of small z (left) and large z (right).

When $\xi/2 \le \Delta < \xi$, the only even-numbered layers overlapping with the sphere of radius ξ are still B_2 and B_{2M}, but now the shape of the overlapping region may, depending on z, be either a one- or a two-base spherical segment. Focusing first on the overlapping region above the center of the sphere, this is a one-base spherical segment of height $z + \xi - \Delta$ for $0 \le z \le 2\Delta - \xi$ (see Fig. 17, left) and a two-base spherical segment of height Δ and radii $\overline{\mathrm{AE}} = \sqrt{\xi^2 - (2\Delta - z)^2}$ and $\overline{\mathrm{BF}} = \sqrt{\xi^2 - (\Delta - z)^2}$ for $z > 2\Delta - \xi$ (see Fig. 17, right). Similarly, the overlapping region below the sphere center is a two-base spherical segment of height Δ and radii $\overline{\mathrm{CE}} = \sqrt{\xi^2 - z^2}$ and $\overline{\mathrm{DF}} = \sqrt{\xi^2 - (z + \Delta)^2}$ for $z < \xi - \Delta$ (see Fig. 17, left) and a one-base spherical segment of height $\xi - z$ for $\xi - \Delta \le z \le \Delta$ (see Fig. 17, right). Since the volume of a two-base spherical segment of height h and radii r_1 and r_2 is $\pi h(r_1^2 + r_2^2)/2 + \pi h^3/6$, we finally obtain

$$\begin{aligned}\int_0^{\Delta} \mathrm{d}z\, \mathscr{V}(z) &= \pi \int_0^{2\Delta-\xi} \mathrm{d}z\, (z + \xi - \Delta)^2 \left(\xi - \frac{z + \xi - \Delta}{3}\right) \\ &+ \pi \int_{2\Delta-\xi}^{\Delta} \mathrm{d}z \left\{\frac{\Delta}{2}\left[2\xi^2 - (\Delta - z)^2 - (2\Delta - z)^2\right] \right. \\ &\left. + \frac{1}{6}\Delta^3\right\} + \pi \int_0^{\xi-\Delta} \mathrm{d}z \left\{\frac{\Delta}{2}\left[2\xi^2 - z^2 - (z + \Delta)^2\right] \right. \\ &\left. + \frac{1}{6}\Delta^3\right\} + \pi \int_{\xi-\Delta}^{\Delta} \mathrm{d}z\, (\xi - z)^2 \left(\xi - \frac{\xi - z}{3}\right) \\ &= \pi\left(-\frac{\xi^4}{2} + \frac{8}{3}\xi^3\Delta - 2\xi^2\Delta^2 + \frac{1}{3}\Delta^4\right). \end{aligned} \tag{B2}$$

We have verified that the two expressions of Eq. (29) for $\xi/2 \le \Delta < \xi$ and $\Delta \ge \xi$ join smoothly (i.e., with continuous first- and second-order derivatives) for $\Delta = \xi$.

Finally, when Δ is smaller than $\xi/2$, the possible overlapping geometries are more numerous. However, the cases already considered are sufficient for our purposes (see main text), and no other calculation is then needed.

REFERENCES

[1] S. C. Glotzer and M. J. Solomon, Nat. Mater. **6**, 557 (2007).
[2] Q. Chen, S. C. Bae, and S. Granick, Nature **469**, 381 (2011).
[3] S. Sacanna and D. J. Pine, Curr. Opin. Colloid Interface Sci. **16**, 96 (2011).
[4] W. Li, H. Palis, R. Merindol, J. Majimel, S. Ravaine, and E. Duguet, Chem. Soc. Rev. **49**, 1955 (2020).
[5] S. C. Glotzer, M. J. Solomon, and N. A. Kotov, AIChE J. **50**, 2978 (2004).
[6] F. Sciortino and E. Zaccarelli, Curr. Opin. Solid State Mater. Sci. **15**, 246 (2011).
[7] S. Sacanna, M. Korpics, K. Rodriguez, L. Colón-Meléndez, S. H. Kim, D. J. Pine, and G. R. Yi, Nat. Commun. **4**, 1688 (2013).
[8] M. Fialkowski, A. Bitner, and B. A. Grzybowski, Nat. Mater. **4**, 93 (2005).
[9] F. Lo Verso, A. Z. Panagiotopoulos, and C. N. Likos, Phys. Rev. E **79**, 010401 (2009).
[10] G. Munaò, A. De Nicola, F. Müller-Plathe, T. Kawakatsu, A. Kalogirou, and G. Milano, Macromolecules **52**, 8826 (2019).
[11] Q. Meng, Y. Kou, X. Ma, Y. Liang, L. Guo, C. Ni, and K. Liu, Langmuir **28**, 5017 (2012).
[12] G. Rosenthal, K. E. Gubbins, and S. H. Klapp, J. Chem. Phys. **136**, 174901 (2012).
[13] T. Kato, Science **295**, 2414 (2002).
[14] C. Tschierske, Angew. Chem., Int. Ed. **52**, 8828 (2013).
[15] R. P. Sear, Curr. Opin. Colloid Interface Sci. **11**, 35 (2006).
[16] J. J. McManus, P. Charbonneau, E. Zaccarelli, and N. Asherie, Curr. Opin. Colloid Interface Sci. **22**, 73 (2016).
[17] J. Hou, M. Li, and Y. Song, Nano Today **22**, 132 (2018).
[18] H. Mohwald, Thin Solid Films **159**, 1 (1988).
[19] S. L. Keller and H. M. McConnell, Phys. Rev. Lett. **82**, 1602 (1999).
[20] P. Akcora *et al.*, Nat. Mater. **8**, 354 (2009).
[21] G. Munaò, A. Pizzirusso, A. Kalogirou, A. De Nicola, T. Kawakatsu, F. Müller-Plathe, and G. Milano, Nanoscale **10**, 21656 (2018).
[22] W. Selke, Phys. Rep. **170**, 213 (1988).
[23] G. Malescio and G. Pellicane, Nat. Mater. **2**, 97 (2003).
[24] G. Malescio and G. Pellicane, Phys. Rev. E **70**, 021202 (2004).
[25] H. Pattabhiraman and M. Dijkstra, Soft Matter **13**, 4418 (2017).
[26] Y. D. Fomin, E. N. Tsiok, and V. N. Ryzhov, Physica A **527**, 121401 (2019).
[27] F. Sciortino, S. Mossa, E. Zaccarelli, and P. Tartaglia, Phys. Rev. Lett. **93**, 055701 (2004).
[28] J. C. F. Toledano, F. Sciortino, and E. Zaccarelli, Soft Matter **5**, 2390 (2009).
[29] D. Costa, C. Caccamo, J.-M. Bomont, and J.-L. Bretonnet, Mol. Phys. **109**, 2845 (2011).
[30] J.-M. Bomont and D. Costa, J. Chem. Phys. **137**, 164901 (2012).
[31] Y. Zhuang and P. Charbonneau, J. Phys. Chem. B **120**, 7775 (2016).
[32] P. D. Godfrin, N. E. Valadez-Perez, R. Castañeda-Priego, N. Wagner, and Y. Liu, Soft Matter **10**, 5061 (2014).
[33] D. McDermott, C. J. Olson Reichhardt, and C. Reichhardt, Soft Matter **10**, 6332 (2014).
[34] Y. Zhuang, K. Zhang, and P. Charbonneau, Phys. Rev. Lett. **116**, 098301 (2016).
[35] D. Pini and A. Parola, Soft Matter **13**, 9259 (2017).
[36] D. Pini, Soft Matter **14**, 6595 (2018).

[37]G. Munaò, S. Prestipino, J. M. Bomont, and D. Costa, J. Phys. Chem. B **126**, 2027 (2022).
[38]S. Das, E.-S. M. Duraia, O. D. Velev, M. D. Amiri, and G. W. Beall, Appl. Surf. Sci. **435**, 512 (2018).
[39]K. Khalil, A. Sagastegui, Y. Li, M. A. Tahir, J. E. S. Socolar, B. J. Wiley, and B. B. Yellen, Nat. Commun. **3**, 794 (2012).
[40]C. I. Mendoza and E. Batta, Europhys. Lett. **85**, 56004 (2009).
[41]A. Ciach, Mol. Phys. **109**, 1101 (2011).
[42]L. A. Padilla, A. A. León-Islas, J. Funkhouser, J. C. Armas-Pèrez, and A. Ramìrez-Hernández, J. Chem. Phys. **155**, 214901 (2021).
[43]O. Patsahan, M. Litniewski, and A. Ciach, Soft Matter **17**, 2883 (2021).
[44]G. Munaò, D. Costa, G. Malescio, J. M. Bomont, and S. Prestipino, Soft Matter **18**, 6453 (2022).
[45]A. Ciach, A. De Virgiliis, A. Meyra, and M. Litniewski, Molecules **28**, 1366 (2023).
[46]G. Munaò, D. Costa, G. Malescio, J. M. Bomont, and S. Prestipino, Phys. Chem. Chem. Phys. **25**, 16227 (2023).
[47]D. Costa, G. Munaò, J.-M. Bomont, G. Malescio, A. Palatella, and S. Prestipino, Phys. Rev. E **108**, 034602 (2023).
[48]D. Pini, A. Parola, and L. Reatto, J. Chem. Phys. **143**, 034902 (2015).
[49]C. N. Likos, A. Lang, M. Watzlawek, and H. Löwen, Phys. Rev. E **63**, 031206 (2001).
[50]N. B. Wilding, F. Schmid, and P. Nielaba, Phys. Rev. E **58**, 2201 (1998).
[51]D. Pini, M. Tau, A. Parola, and L. Reatto, Phys. Rev. E **67**, 046116 (2003).
[52]A. J. Archer, C. Ionescu, D. Pini, and L. Reatto, J. Phys.: Condens. Matter **20**, 415106 (2008).
[53]P. Tarazona, Phys. Rev. A **31**, 2672 (1985).
[54]P. Tarazona, Phys. Rev. A **32**, 3148 (1985).
[55]A. R. Denton and N. W. Ashcroft, Phys. Rev. A **39**, 4701 (1989).
[56]Y. Rosenfeld, Phys. Rev. Lett. **63**, 980 (1989).
[57]G. Foffi, G. D. McCullagh, A. Lawlor, E. Zaccarelli, K. A. Dawson, F. Sciortino, P. Tartaglia, D. Pini, and G. Stell, Phys. Rev. E **65**, 031407 (2002).
[58]K. R. Hall, J. Chem. Phys. **57**, 2252 (1972).
[59]D. Frenkel and B. Smit, *Understanding Molecular Simulations*, 2nd ed. (Academic Press, New York, 2002).
[60]P. J. Steinhardt, D. R. Nelson, and M. Ronchetti, Phys. Rev. B **28**, 784 (1983).
[61]P. R. ten Wolde, M. J. Ruiz-Montero, and D. Frenkel, J. Chem. Phys. **104**, 9932 (1996).
[62]S. Prestipino, J. Chem. Phys. **148**, 124505 (2018).
[63]S. Prestipino and P. V. Giaquinta, J. Stat. Mech.: Theory Exp. **2004**(09), P09008.
[64]S. Prestipino and P. V. Giaquinta, Entropy **22**, 1024 (2020).
[65]J. M. Polson and D. Frenkel, Phys. Rev. E **56**, R6260 (1997).
[66]K. Binder, B. J. Block, P. Virnau, and A. Tröster, Am. J. Phys. **80**, 1099 (2012).
[67]S. Prestipino, C. Caccamo, D. Costa, G. Malescio, and G. Munaò, Phys. Rev. E **92**, 022141 (2015).
[68]M. C. Abramo, C. Caccamo, D. Costa, P. V. Giaquinta, G. Malescio, G. Munaò, and S. Prestipino, J. Chem. Phys. **142**, 214502 (2015).
[69]H. Liu, S. Garde, and S. Kumar, J. Chem. Phys. **123**, 174505 (2005).
[70]D. L. Pagan and J. D. Gunton, J. Chem. Phys. **122**, 184515 (2005).
[71]J. Largo, M. A. Miller, and F. Sciortino, J. Chem. Phys. **128**, 134513 (2008).